

Electronic structures of (In,Ga)As/GaAs quantum dot molecules made of dots with dissimilar sizes

Lixin He¹ and Alex Zunger²

¹Key Laboratory of Quantum Information, University of Science and Technology of China, Hefei, Anhui 230026, Peoples Republic of China

²National Renewable Energy Laboratory, Golden, Colorado 80401, USA

(Dated: September 19, 2018)

Using single-particle pseudopotential and many-particle configuration interaction methods, we compare various physical quantities of (In,Ga)As/GaAs quantum dot molecules (QDMs) made of dissimilar dots (heteropolar QDMs) with QDMs made of identical dots (homopolar QDMs). The calculations show that the electronic structures of hetero-QDMs and homo-QDMs differ significantly at large inter-dot distance. In particular (i) Unlike those of homo-QDMs, the single-particle molecular orbitals of hetero-QDMs convert to dot localized orbitals at large inter-dot distance. (ii) Consequently, in a hetero-QDM the bonding-antibonding splitting of molecular orbitals at large inter-dot distance is significantly larger than the electron hopping energy whereas for homo-QDM, the bonding-antibonding splitting is very similar to the hopping energy. (iii) The asymmetry of the QDM increases significantly the double occupation for the two-electron ground states, and therefore lowers the degree of entanglement of the two electrons.

PACS numbers: 73.22.GK, 03.67.Mn, 85.35.-p

I. INTRODUCTION

Vertically coupled quantum dots^{1,2} obtained via epitaxial growth provide a potential scheme for scalable nano-structures for quantum computing. In this scheme, two coupled quantum dots are used as a basic logic gate, via the entanglement of one exciton³ or two electronic spins.⁴ This proposal for gate operations, requires knowledge of the detailed physical properties of the “quantum gate” made of two quantum dots. Significant progress has been recently made^{5,6} using quantum dot molecules made of very large (~ 500 - 1000 Å) electrostatically confined dots. The limit of large quantum confinement, however, requires working with (200×30 Å) self-assembled QDMs. So far, most experiments on self-assembled QDM are optical,³ and most theories are based on continuum models, such as effective mass approximations.³ These simple models ignore or drastically simplify important real material properties such as strain, atomistic symmetries and crystal structural effects, band coupling etc. Recent studies⁷ show that simplification of such important effects may lead to qualitative changes in fundamental physics of the QDMs.

Previously, we have studied homopolar QDMs made of two identical quantum dots, using single-particle pseudopotential method and many-particle configuration interaction method.^{8,9} We have studied electron localization, double occupation rate and two-electron entanglement using a new formula for measuring the degree of entanglement formula for two *indistinguishable* fermions. We found that even geometrically identical dots in the QDMs lead to electronic asymmetry due to the strain effects. However, experimentally it is hard to control the shape, size and compositions of individual dots within the QDMs, so in practice, the QDMs are never made of identical dots. Actually, the top dots are tend to be larger

than the bottom dots due to the strain effects.^{1,2} Indeed, the measured difference in exciton energy due to dot-size difference is about 4 meV¹⁰ for two vertically coupled dots that are 20 nm apart. Sometimes, the two dots are intentionally grown different so that they can be addressed separately.¹¹ To provide quantitative comparison to experiments, considering the effects that asymmetry of quantum dots within the molecule, we studied the QDMs made of (In,Ga)As/GaAs quantum dots of different sizes (hetero-polar QDM).

In this paper, we study systematically the electronic properties of hetero-QDMs, including their single-particle molecular orbitals, many-particle states, double occupation and entanglement of two-electrons, and compare them to those of homo-QDMs. We found that while at *short* inter-dot distance, the electronic properties of hetero-QDM and homo-QDM are similar, they differ significantly at *large* inter-dot distance. This difference may have substantial impact in implementation of quantum gates.

II. METHODS

Figure 1 shows the geometry of a hetero-QDM, consisting a pair of 3 nm tall InAs dots in the shape of truncated cones, grown on two-dimensional InAs wetting layers, embedded in a GaAs matrix. The inter-dot separation d is defined as the distance between the wetting layers of top and bottom dots. We choose the base diameter of top dots (labeled as α) to be 20 nm, and that of the bottom dots (labeled as β) to be 19 nm, mimicking to the fact that experimentally the top dots are slightly larger than the bottom dots.^{1,2,10} The composition of the dots vary from In_{0.5}Ga_{0.5}As at their bases to pure InAs at their top, as determined in Ref. 3. We de-

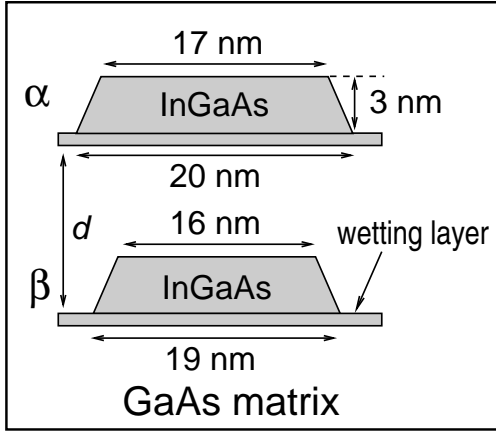


FIG. 1: The geometry used in this work for quantum dot molecules made of dissimilar dots. We denote the (isolated) top dot “ α ” and the (isolated) bottom dot “ β ”. Each dot has the shape of a truncated cone. The inter-dot distance is measured from wetting layer to wetting layer.

note the dot molecules made of dissimilar dots α and β as $M_{\alpha\beta}$. We also constructed the homo-QDM, consisting a pair of quantum dots γ , which have the average sizes, and the same alloy compositions of dots α and β in the heteropolar dot molecule. We denote the homo-QDM as $M_{\gamma\gamma}$.

The single-particle energy levels and wavefunctions of $M_{\alpha\beta}$ and $M_{\gamma\gamma}$ are obtained by solving the Schrödinger equations in a pseudopotential scheme,

$$\left[-\frac{1}{2} \nabla^2 + V_{\text{ps}}(\mathbf{r}) \right] \psi_i(\mathbf{r}) = \epsilon_i \psi_i(\mathbf{r}), \quad (1)$$

where the total electron-ion potential $V_{\text{ps}}(\mathbf{r})$ is a superposition of local, screened atomic pseudopotentials $v_\alpha(\mathbf{r})$, and a nonlocal spin-orbit potential V_{so} i.e., $V_{\text{ps}}(\mathbf{r}) = \sum_{n,\alpha} v_\alpha(\mathbf{r} - \mathbf{R}_{n,\alpha}) + V_{\text{so}}$. The atomic position $\{\mathbf{R}_{n,\alpha}\}$ is obtained from minimizing the total bond-bending and bond-stretching energy using the Valence Force Field (VFF) model.^{12,13} The atomistic pseudopotentials v_α ($\alpha = \text{In, Ga, As}$) are fitted to the physically important quantities of bulk InAs and GaAs, including band energies, band-offsets, effective masses, deformation potentials and alloy bowing parameters, etc.¹⁴ Because for electrons the spin-orbit coupling is extremely small in the InAs/GaAs quantum dots, we ignored this effect. In general, including the spin-orbit coupling effect will introduce mixture of different total spin states. Equation (1) is solved in the basis of $\{\phi_{m,\vec{\epsilon},\lambda}(\mathbf{k})\}$ of Bloch orbitals of band index m and wave vector \mathbf{k} of material λ (= InAs, GaAs), strained uniformly to strain $\vec{\epsilon}$ following Ref. 15.

The Hamiltonian of interacting electrons can be written as,

$$H = \sum_{i\sigma} \epsilon_\alpha \hat{\psi}_{i\sigma}^\dagger \hat{\psi}_{i\sigma} + \frac{1}{2} \sum_{ijkl} \sum_{\sigma,\sigma'} \Gamma_{k,l}^{i,j} \hat{\psi}_{i\sigma}^\dagger \hat{\psi}_{j\sigma'}^\dagger \hat{\psi}_{k\sigma'} \hat{\psi}_{l\sigma}, \quad (2)$$

where $\hat{\psi}_{i\sigma}(\mathbf{r}) = c_{i\sigma} \psi_{i\sigma}(\mathbf{r})$ is the field operator, whereas

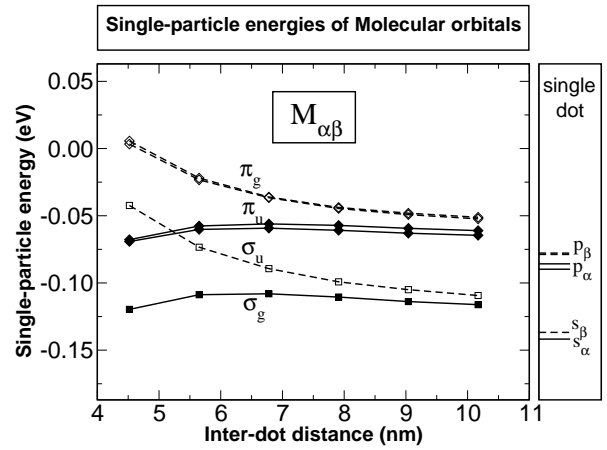


FIG. 2: Left panel: The single-particle energy levels of molecular orbitals *vs.* inter-dot distance. Right panel: The electron single-particle energy levels of the isolated dots α and β .

$c_{i\sigma}$ is a fermion operator. $\psi_i = \sigma_u, \sigma_g, \pi_u, \pi_g$ are the single-particle eigenfunctions of the i -th molecular orbital, and $\sigma, \sigma' = 1, 2$ are spin indices. The Γ_{kl}^{ij} are the Coulomb integrals between molecular orbitals ψ_i, ψ_j, ψ_k and ψ_l ,

$$\Gamma_{kl}^{ij} = \int \int d\mathbf{r} d\mathbf{r}' \frac{\psi_i^*(\mathbf{r}) \psi_j^*(\mathbf{r}') \psi_k(\mathbf{r}') \psi_l(\mathbf{r})}{\epsilon(\mathbf{r} - \mathbf{r}') |\mathbf{r} - \mathbf{r}'|}. \quad (3)$$

The $J_{ij} = \Gamma_{ji}^{ij}$ and $K_{ij} = \Gamma_{ij}^{ij}$ are diagonal Coulomb and exchange integrals respectively. The remaining terms are called off-diagonal or scattering terms. All Coulomb integrals are calculated numerically from atomistic wavefunctions.¹⁶ We use a phenomenological, position-dependent dielectric function $\epsilon(\mathbf{r} - \mathbf{r}')$ to screen the electron-electron interaction.¹⁶ The many-particle problem of Eq.(2) is solved via the CI method, by expanding the N -electron wavefunction in a set of Slater determinants, $|\Phi_{e_1, e_2, \dots, e_N}\rangle = c_{e_1}^\dagger c_{e_2}^\dagger \dots c_{e_N}^\dagger |\Phi_0\rangle$, where $c_{e_i}^\dagger$ creates an electron in the state e_i . The ν -th many-particle wavefunction is then the linear combinations of the determinants,

$$|\Psi_\nu\rangle = \sum_{e_1, e_2, \dots, e_N} A_\nu(e_1, e_2, \dots, e_N) |\Phi_{e_1, e_2, \dots, e_N}\rangle. \quad (4)$$

For the two-electron problems, our calculations include all possible Slater determinants of six confined molecular orbitals.

III. BASIC ELECTRONIC STRUCTURES AT THE SINGLE-PARTICLE LEVEL

A. Double-dot molecular orbitals

We first show the electronic structure of isolated dots α and β . The single-dot electron s and p levels of dots α

and β are shown on the right panel of Fig. 2. We see that the s - p energy spacing of dot α is $\epsilon(p_\alpha) - \epsilon(s_\alpha) = 52$ meV and that of dot β is $\epsilon(p_\beta) - \epsilon(s_\beta) = 59$ meV, compared to 54 meV of dot γ (not shown). The energy level of s_β , is slightly (~ 6 meV) higher than s_α , because dot β is smaller than dot α and therefore has larger confinement. The p levels of all dots have a small energy splitting due to the underlying atomistic symmetry, e.g., $\delta\epsilon(p_\alpha) = 6$ meV, and $\delta\epsilon(p_\beta) = 1$ meV. We further calculated the fundamental exciton energy of dot α , $E_X(\alpha) = 1153$ meV, and that of dot β , $E_X(\beta) = 1159$ meV. The energy difference in exciton of dots α and β is about 6 meV, in agreement with experiment.¹⁰ The fundamental exciton energy of the “averaged” dot γ is $E_X(\gamma) = 1156$ meV.

When two dots α and β couple, the bonding and anti-bonding “molecular orbitals” ensue from the single-dot orbitals. The energy levels of molecular orbitals are shown on the left panel of Fig. 2. We show the single-particle levels of molecular orbitals^{8,9} σ_g , σ_u originating from s orbitals, and π_u , and π_g originating from p orbitals. The bonding and anti-bonding splitting $\Delta_\sigma = \epsilon(\sigma_u) - \epsilon(\sigma_g)$ and $\Delta_\pi = \epsilon(\pi_g) - \epsilon(\pi_u)$ increase with the decrease of inter-dot distance, because the coupling between the top and bottom dots gets stronger. This picture is similar to what we obtained for homo-QDMs. However, there is an important difference between the homo-QDMs $M_{\gamma\gamma}$ and hetero-QDMs $M_{\alpha\beta}$: in the former case, the bonding and anti-bonding splitting Δ_σ and Δ_π decay to almost zero at large inter-dot distance, while in the later case, Δ_σ and Δ_π tend to constants ($\Delta_\sigma \sim 7$ meV, $\Delta_\pi \sim 10$ meV here), because the molecular orbitals gradually convert at large inter-dot distance to single dot energy levels, e.g. the σ_g levels convert to top dot s orbitals, and σ_u convert to bottom dot s orbitals, therefore the energy splitting between the first and second molecular states at large distances is approximately the energy difference between s orbitals of the top and bottom dots, i.e., $\Delta_\sigma \sim \epsilon(s_\beta) - \epsilon(s_\alpha) \neq 0$ for $M_{\alpha\beta}$.

Figure 2 shows that at inter-dot distance $d = 10$ nm, the molecular orbital levels are about 25 meV higher than the isolated dot levels, although the direct electronic coupling between two dots is much smaller than this quantity. This energy shift results from the long range strain effects experienced by one dot due to the presence of the second dots. This effect is missed in EMA-type model calculations,¹⁷ which ignore strain effects.

B. Single dot-localized orbitals

The above discussions pertain to the basis of double-dot molecular orbitals. An alternative way to study QDMs is to use a dot-localized basis. We have demonstrated^{8,9} that dot-localized orbitals can be a useful tool to analyze the QDM physics, including the electron double occupation, and two-electron entanglement.

Dot-localized orbitals χ_η can be obtained from a uni-

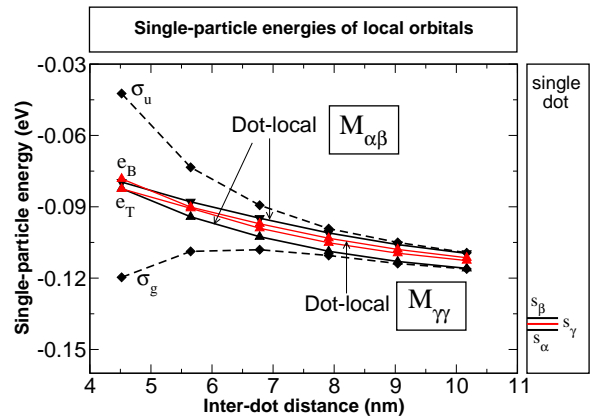


FIG. 3: (Color online) Left panel: The energy levels of dot-localized orbitals for QDMs $M_{\alpha\beta}$ (black solid lines) and $M_{\gamma\gamma}$ (red solid lines). e_T and e_B denote the s orbitals of the top and bottom dots respectively. The molecular orbitals energy levels σ_g and σ_u (dashed lines) are shown for dot molecules $M_{\alpha\beta}$. Right panel: s levels of *isolated* dots α , β and γ .

tary rotation of molecular orbitals, i.e.,

$$\chi_\eta = \sum_{i=1}^N \mathcal{U}_{\eta,i} \psi_i, \quad (5)$$

where, ψ_i is the i -th molecular orbital, and \mathcal{U} is a unitary matrix, i.e., $\mathcal{U}^\dagger \mathcal{U} = I$. We choose the unitary matrices \mathcal{U} that maximize the total orbital self-Coulomb energy.^{9,18} The procedure of finding \mathcal{U} is described in the Appendix B of Ref.9. As we will show below these dot-localized orbitals χ_η have the advantage of being only weakly dependant to the inter-dot coupling. This invariance may provide simplified pictures for qualitatively understanding of the QDM physics.

1. Single-particle energies of dot-localized orbitals

The single-particle levels of dot-localized orbitals and the hopping (or tunneling) term between two dots can be obtained from

$$e_\eta = \langle \chi_\eta | \hat{H}_0 | \chi_\eta \rangle = \sum_i \mathcal{U}_{\eta,i}^* \mathcal{U}_{\eta,i} \epsilon_i, \quad (6)$$

$$t_{\eta_1 \eta_2} = \langle \chi_{\eta_1} | \hat{H}_0 | \chi_{\eta_2} \rangle = \sum_i \mathcal{U}_{\eta_1,i}^* U_{\eta_2,i} \epsilon_i, \quad (7)$$

where, ϵ_i is the single-particle energy of i -th molecular orbital and $\hat{H}_0 = \sum_{i\sigma} \epsilon_i \hat{\psi}_{i\sigma}^\dagger \hat{\psi}_{i\sigma}$ is the single-particle Hamiltonian. Figure 3 depicts the single-particle levels e_T and e_B of the dot-localized orbitals of both top and bottom dots, for inter-dot distances d in the range from 4 nm to 10 nm. (Here, we denote the top dot T and the bottom dot B , to distinguish them from isolated dots α , β and γ). e_T and e_B of $M_{\alpha\beta}$ are shown in the black

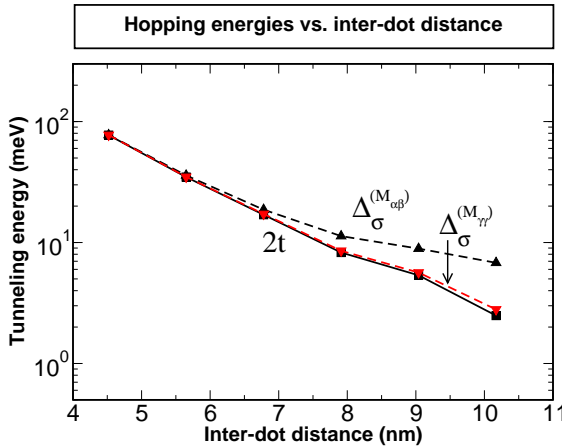


FIG. 4: (Color online) The inter-dot hopping energy $2t$ (solid lines) of hetero-QDM $M_{\alpha\beta}$ and homo-QDM $M_{\gamma\gamma}$. We also show the bonding-antibonding splitting Δ_σ of $M_{\alpha\beta}$ and $M_{\gamma\gamma}$

solid lines, and those of $M_{\gamma\gamma}$ are shown in the red solid lines. At large d , the energy difference $e_B - e_T \sim 6$ meV for $M_{\alpha\beta}$, is close to the value of difference $\epsilon(s_\beta) - \epsilon(s_\alpha)$ between s orbitals of isolated dots α, β . This energy difference gets smaller when the two dots move closer, because the energy levels of the top dot rise faster than those of bottom dots due to the strain asymmetry. For the homo-QDMs $M_{\gamma\gamma}$, e_T and e_B are almost degenerate. The small difference (~ 1 meV) between them is due to the strain and alloy effects. We also plot in Fig. 3 the energies of molecular orbitals σ_u and σ_g in dashed lines for $M_{\alpha\beta}$. As we see, for $d > 9$ nm, the dot-localized state e_B of $M_{\alpha\beta}$ is almost identical to the molecular orbital σ_u , while e_T merges with σ_g , indicating at large d , molecular orbitals convert to dot-centered orbitals for $M_{\alpha\beta}$.

The quantity $2t$ measures the coupling strength between the top and bottom dots, and directly determines the two-electron properties such as singlet-triplet splitting in the QDM. We calculate this hopping energy between the s orbitals of top and bottom dots at different inter-dot distances for both $M_{\alpha\beta}$ and $M_{\gamma\gamma}$ in Fig. 4. (We ignore the orbital index “ s ” to simplify the notation.) We find that $2t(M_{\alpha\beta})$ and $2t(M_{\gamma\gamma})$ are almost identical at all inter-dot distance. However, the hopping energies calculated here are much larger than we obtained for the pure InAs/GaAs QDM⁹, because the alloy QDM have much smaller energy barrier between two dots than pure QDM. In general, the quantity $2t$ does not equal to the bonding-antibonding splitting $\Delta_\sigma = \sqrt{\delta^2 + 4t^2}$, where $\delta = \epsilon(e_T) - \epsilon(e_B)$, being the energy difference of s orbitals of the top and bottom dots. For homo-QDMs, where $\delta/2t \ll 1$, we have $2t \sim \Delta_\sigma$ as seen in Fig. 4. However, for hetero-QDMs, Δ_σ may be significantly different from $2t$, especially at *large* inter-dot distances, where $\delta/2t \gg 1$, also illustrated in Fig. 4. Experimentally,¹⁹ one usually measures the bonding-antibonding splitting

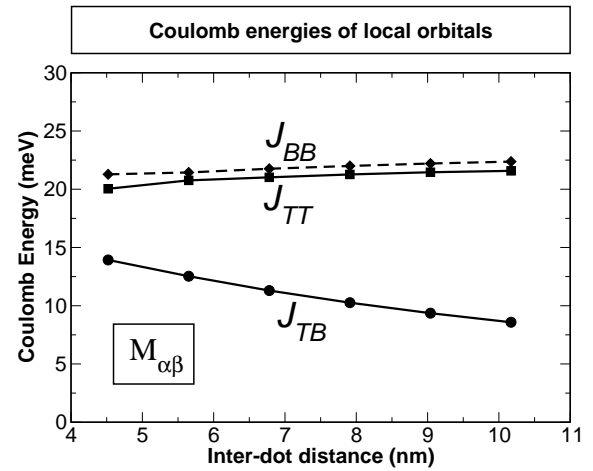


FIG. 5: The Coulomb energies of dot-localized orbitals of hetero-QDM $M_{\alpha\beta}$. J_{TT} and J_{BB} are the s orbital self-Coulomb energies of top and bottom dots respectively, whereas J_{TB} are the Coulomb energies between s orbitals of the top and the bottom dots.

rather than the hopping $2t$. Therefore, to get the hopping energy between two dots, one need to know the energy difference δ of two dots.

2. Coulomb integrals of dot-localized orbitals

The Coulomb integrals in the dot-localized basis can be obtained from Coulomb integrals of molecular orbitals as follows,

$$\tilde{\Gamma}_{\eta_3, \eta_4}^{\eta_1, \eta_2} = \sum_{i, j, k, l} \mathcal{U}_{\eta_1, i}^* \mathcal{U}_{\eta_2, j}^* \mathcal{U}_{\eta_3, k} \mathcal{U}_{\eta_4, l} \Gamma_{k, l}^{i, j}, \quad (8)$$

where $\Gamma_{k, l}^{i, j}$ are the Coulomb integrals in the molecular basis. The direct Coulomb integrals J_{TT} , J_{BB} and J_{TB} for $M_{\alpha\beta}$ are shown in Fig. 5. The Coulomb integrals $J_{TT} \sim J_{\alpha\alpha} = 21.4$ meV and $J_{BB} \sim J_{\beta\beta} = 22.3$ meV, are almost constants at all inter-dot distances, suggesting that the dot-localized orbitals are approximately unchanged for different inter-dot distance d . $J_{\beta\beta} > J_{\alpha\alpha}$, as dot β is smaller than dot α . The inter-dot Coulomb interaction J_{TB} decay slowly as $1/d$. The exchange energies (not shown) between the top and bottom electrons is orders of magnitude smaller than the hopping energy, and therefore can be ignored in practice. For the homo-QDM $M_{\gamma\gamma}$, we found that on-site Coulomb energies $J_{TT} \sim J_{BB}$, both are very close to the average values of J_{TT} and J_{BB} of $M_{\alpha\beta}$. The inter-dot Coulomb energies J_{TB} of $M_{\alpha\beta}$ and $M_{\gamma\gamma}$ are also extremely close.

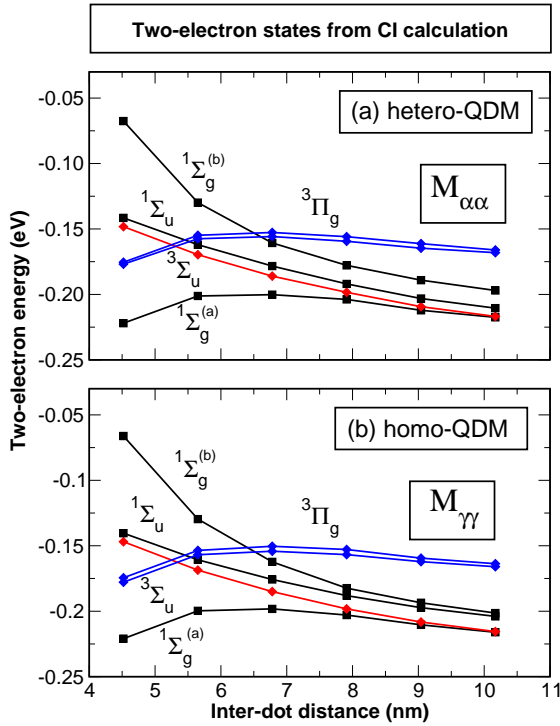


FIG. 6: (Color online) Two-electron states for (a) hetero-QDM $M_{\alpha\beta}$ and (b) homo-QDM $M_{\gamma\gamma}$, including the singlet $^1\Sigma_g^{(a)}$, $^1\Sigma_u$, $^1\Sigma_g^{(b)}$ states and the 3-fold degenerated triplet states $^3\Sigma_u$ as well as two 3-fold degenerated triplet states $^3\Pi_u$.

IV. TWO ELECTRONS IN THE DOT MOLECULE

A. Many-body energy states

The two-electron-in-a-QDM problem is of special interest, as it is the prototype of quantum gate using QDMs.⁴ We calculate the two-electron energy levels by the configuration interaction method using Slater determinants constructed from confined molecular orbitals σ_g , σ_u and π_u , π_g , which give 66 configurations in total. The two-electron energies Σ and $^3\Pi_u$ for hetero-QDMs $M_{\alpha\beta}$ are plotted in Fig. 6(a). To compare with homo-QDMs, we show the two-electron states of $M_{\gamma\gamma}$ in Fig. 6(b). The energy levels of $M_{\alpha\beta}$ are similar to those of $M_{\gamma\gamma}$, in the following way: (i) The order of the CI levels is unchanged, particularly the ground states are still the singlet states $^1\Sigma_g^{(a)}$ at all inter-dot distance; (ii) The trend of each CI level vs. inter-dot distance d is similar to what we obtained for $M_{\gamma\gamma}$. There are also some differences between the hetero-QDMs $M_{\alpha\beta}$ and homo-QDMs $M_{\gamma\gamma}$, especially at larger inter-dot distances. For example, in the homopolar QDMs, the $^1\Sigma_u$ state is almost degenerate with $^1\Sigma_g^{(b)}$ at large inter-dot distance, while in $M_{\alpha\beta}$, $^1\Sigma_g^{(b)}$ is about 13 meV higher than $^1\Sigma_u$ at $d=10$ nm. At large d , $^1\Sigma_u$ and $^1\Sigma_g^{(b)}$ correspond to the states that two electrons

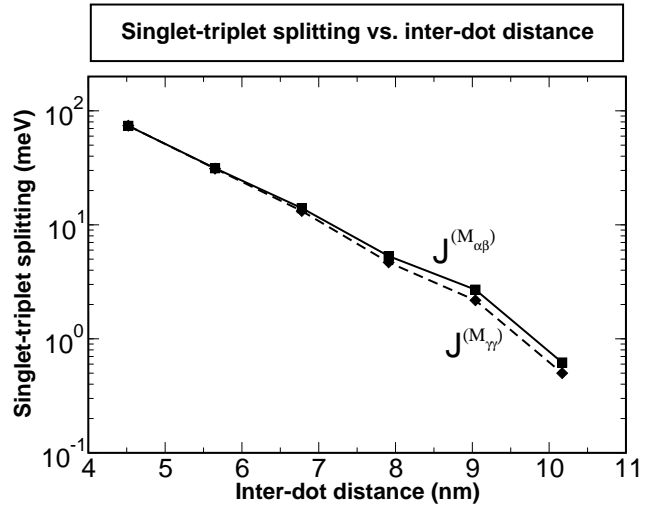


FIG. 7: The singlet-triplet splitting J_{S-T} vs. inter-dot distance for hetero-QDM $M_{\alpha\beta}$ (solid line) and homo-QDM $M_{\gamma\gamma}$ (dashed line).

localized on the same dots.^{8,9} The energy difference between $^1\Sigma_g^{(b)}$ and $^1\Sigma_u$ is due to the size difference of dots α and β .

The singlet $^1\Sigma_g^{(a)}$ and triplet states $^3\Sigma$ can be used as two qubit states in quantum computing. In a proposed quantum SWAP gate,⁴ the gate operation time $\tau \sim 1/J_{S-T}$, where J_{S-T} being the singlet-triplet energy splitting. The singlet-triplet splitting of $M_{\alpha\beta}$ is shown in Fig. 7 on a semi-log plot. We see that it decay approximately exponentially with the inter-dot distance. We also show in Fig. 7 the singlet-triplet splitting of the homo-QDM $M_{\gamma\gamma}$. We found that the J_{S-T} of homo-QDM $M_{\gamma\gamma}$ is slightly smaller than the J_{S-T} of hetero-QDM $M_{\alpha\beta}$, though the hopping energies of $M_{\alpha\beta}$ and $M_{\gamma\gamma}$ are almost identical. In the hetero-QDM case, the singlet wavefunction has more weight on the lower energy dot and therefore lowers the singlet energy and increases the singlet-triplet splitting.

B. Double occupation of one of the dots in a QDM

Double occupation means that two electrons occupy the same dot in a QDM. If the double occupation rate is high, the quantum gate operation may fail. The double occupation rate also reflects the localization properties of electrons in the QDM. If the double occupation rate is zero, each dot has one electron, whereas double occupation rate of 1 means that two electrons are always localized on a single dot. When the double occupation rate is 0.5, two electrons are delocalized between two dots. The double occupation can be conveniently analyzed in the dot-localized basis by transforming the CI equations to the dot-localized basis.⁸ In the simplest case, we consider only the “s” orbital for each dot, which give six config-

urations as follows, $|e_T^\uparrow, e_B^\uparrow\rangle$, $|e_T^\downarrow, e_B^\downarrow\rangle$, $|e_T^\uparrow, e_B^\downarrow\rangle$, $|e_T^\downarrow, e_B^\uparrow\rangle$, $|e_B^\uparrow, e_B^\downarrow\rangle$ and $|e_T^\uparrow, e_T^\downarrow\rangle$. The Hamiltonian in this basis set

is,⁹

$$H = \begin{pmatrix} e_T + e_B + J_{TB} - K_{TB} & 0 & 0 & 0 & 0 \\ 0 & e_T + e_B + J_{TB} - K_{TB} & 0 & 0 & 0 \\ 0 & 0 & e_T + e_B + J_{TB} - K_{TB} & 0 & 0 \\ 0 & 0 & -K_{TB} & t & t \\ 0 & 0 & e_T + e_B + J_{TB} & -t & -t \\ 0 & 0 & t & 2e_B + J_{BB} & 0 \\ 0 & 0 & t & 0 & 2e_T + J_{TT} \end{pmatrix}. \quad (9)$$

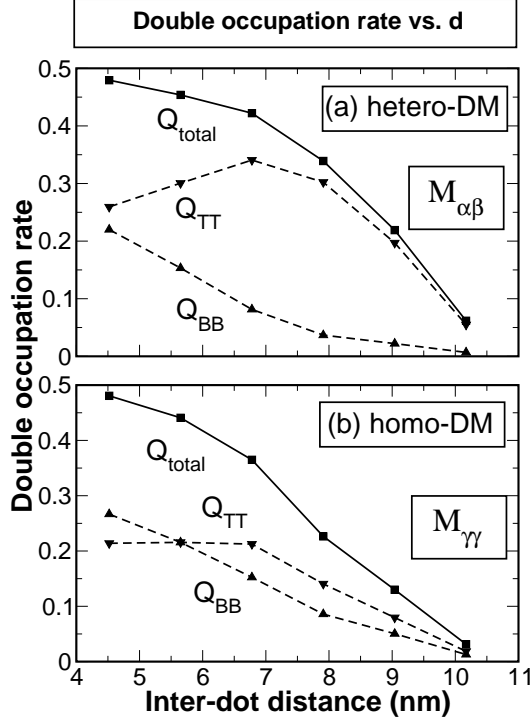


FIG. 8: The double occupation rate of the ground-state singlet ${}^1\Sigma_g^{(a)}$ vs. inter-dot distance for (a) hetero-QDM $M_{\alpha\beta}$ and (b) homo-QDM $M_{\gamma\gamma}$.

where $t = t_{TB}$. We ignored in Eq.(9) the off-diagonal Coulomb integrals, which are much smaller than the hopping t .

The calculation of the matrix elements of Eq. (9) is described in Sec.III B. The two electrons can be either both on the top dots, or both on the bottom dots, or one on the top and the other on the bottom dots. We denote by $\{|\chi_{l,p}^\sigma, \chi_{l',p'}^{\sigma'}\rangle\}$ the configuration where one electron is on the l -th orbital of the p dot with spin σ , and the other electron is on the l' -th orbital of the p' dot with spin σ' . Then the double occupation rate $Q_{pp}^{(\nu)}$ in the many-particle state ν is the probability of two electrons

occupying the dot p = (T or B) at the same time, i.e.,

$$Q_{pp}^{(\nu)} = \sum_{l\sigma, l'\sigma'} P_\nu (|\chi_{l,p}^\sigma, \chi_{l',p'}^{\sigma'}\rangle), \quad (10)$$

where $P_\nu(\mathcal{C})$ is the weight of the configuration \mathcal{C} in the many-body wave functions of state ν . The total probability of two electrons being on the *same* dot is then $Q_{\text{tot}}^{(\nu)} = Q_{\text{TT}}^{(\nu)} + Q_{\text{BB}}^{(\nu)}$ for the ν -th state.

We plot Q_{tot} , Q_{TT} and Q_{BB} of state ${}^1\Sigma_g^{(a)}$ for $M_{\alpha\beta}$ in Fig. 8(a) and for $M_{\gamma\gamma}$ in Fig. 8(b). We also performed calculations on a “symmetrized” model QDM $M_{\alpha'\alpha'}$ by setting $e'_T = e'_B = (e_T + e_B)/2$ and $J'_{TT} = J'_{BB} = (J_{TT} + J_{BB})/2$ of $M_{\alpha\beta}$ in Eq. (9). $M_{\alpha'\alpha'}$ represents an *ideal* homo-QDM, without the asymmetry caused by strain, size and alloy composition effects. When compare the double occupation of the hetero- and homo-QDMs, we see that (i) For both types of QDMs, $Q_{\text{tot}} \sim 0.5$ at $d \sim 4.5$ nm, meaning that two electrons are delocalized on two dots. For both QDMs, Q_{tot} decays monotonically with the inter-dot distance, and at $d \sim 10$ nm, $Q_{\text{tot}} \sim 0$, meaning that the two electrons are about each localized on one of the two dots.

On the other hand, the double occupation of individual dot Q_{TT} and Q_{BB} differ substantially for homo-QDMs and hetero-QDMs:

(ii) For the homo-QDM $M_{\alpha'\alpha'}$, $Q_{\text{BB}} = Q_{\text{TT}}$ and decay monotonically with the inter-dot distances. Q_{BB} and Q_{TT} of $M_{\gamma\gamma}$ have similar features, although Q_{BB} is slightly different from Q_{TT} due to the strain and alloy effects. This feature is also seen in the homo-QDM made of pure InAs/GaAs dots^{8,9}. In the hetero-QDMs $M_{\alpha\beta}$, Q_{TT} behaves very differently from Q_{BB} because the effective single-particle energy $e_T < e_B$. Whereas Q_{BB} decays monotonically with the inter-dot distance, Q_{TT} has a maximum at $d \sim 7$ nm. The reason is that at $d \sim 4.5$ nm, the hopping energy $2t$ is much larger than $e_B - e_T$, therefore the electrons can overcome the energy barrier between the top and bottom dots and distribute evenly between two dots, leading to $Q_{\text{TT}} \sim Q_{\text{BB}}$. At larger d , $2t \ll e_B - e_T$, and the electrons would prefer to localize on the top dots, leading to $Q_{\text{TT}} \gg Q_{\text{BB}}$. Therefore, even when the total double occupation rate drops down, Q_{TT} still increases and reaches the maximum at $d=7$ nm. For $d > 7$ nm, Q_{TT} decays as Q_{tot} decays.

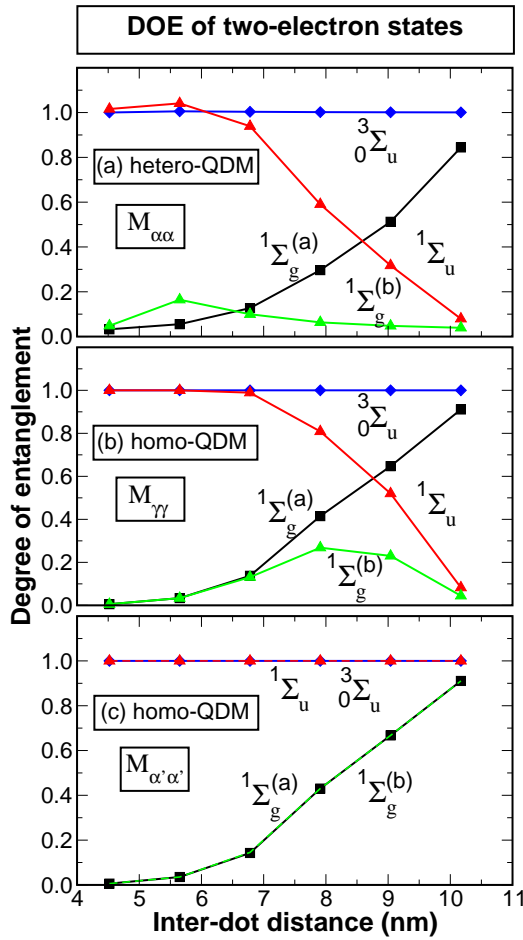


FIG. 9: (Color online) The degree of entanglement of two-electron states $^1\Sigma_g^{(a)}$, $^1\Sigma_u$, $^1\Sigma_g^{(b)}$ and $^3\Sigma_u$, in (a) the hetero-QDM $M_{\alpha\beta}$, (b) the homo-QDM $M_{\gamma\gamma}$ and (c) the model “symmetrized” homo-QDM $M_{\alpha'\alpha'}$.

(iii) The homo-QDMs $M_{\alpha'\alpha'}$ and $M_{\gamma\gamma}$ have almost the same *total* double occupation, both smaller than that of the hetero-QDM $M_{\alpha\beta}$. The asymmetry between two dots increases the total double occupation. In an extreme case, where $e_T \ll e_B$, the two electrons could always localize on the top dots, leading to $Q_{\text{tot}}=Q_{\text{TT}}=1$.

V. ENTANGLEMENT

A. Degree of entanglement for two electrons

The degree of entanglement (DOE) is one of the most important quantities for successful quantum gate operations. For *distinguishable* particles such as an electron and a hole, the DOE can be calculated from the Von Neumann-entropy formulation.^{20,21,22,23} However, Von Neumann entropy formulation can not be used directly to calculate DOE for *indistinguishable* particles.^{24,25,26,27,28,29,30} Schliemann et al. proposed a

quantum correlation function for two electrons which has similar properties as the DOE.²⁴ However, the generalization of this quantum correlation function to a system that has more than two single-particle levels is complicated. We proposed a DOE measure⁹ for indistinguishable fermions using the Slater decompositions^{24,31} as,

$$\mathcal{S} = - \sum_u z_i^2 \log_2 z_i^2, \quad (11)$$

where, z_i are Slater decomposition coefficients and $\sum_i z_i^2 = 1$. As shown in Ref. 9, the DOE measure Eq.(11) reduces to the usual Von Neumann entropy for *distinguishable* particles when the two electrons are far from each other. In Refs. 25,26, a similar DOE measure was defined, which however due to a different normalization condition for z_i was used, does not reduce to the usual Von Neumann entropy even when the two electrons can be distinguished by their sites.

The DOE of Σ states calculated from Eq. (11) for the hetero-QDM $M_{\alpha\beta}$, the homo-QDM $M_{\gamma\gamma}$, and the model homo-QDM $M_{\alpha'\alpha'}$ are shown in Fig. 9(a), (b) and (c) respectively. All of the three QDMs have the following features: (i) $\mathcal{S}(^1\Sigma_g^{(a)})$ is close to zero (unentangled) at $d \sim 4.5$ nm, and close to unity (fully entangled) at $d \sim 10$ nm. (ii) $\mathcal{S}(^3\Sigma_u)$ is almost unity (fully entangled) at all inter-dot distances. However, $\mathcal{S}(^1\Sigma_g^{(a)})$ of the homo-QDM $M_{\gamma\gamma}$ (which is very close the $\mathcal{S}(^1\Sigma_g^{(a)})$ of $M_{\alpha'\alpha'}$) is larger than $\mathcal{S}(^1\Sigma_g^{(a)})$ of the hetero-QDM $M_{\alpha\beta}$, showing that the asymmetry in a QDM lowers the two-electron entanglement of the ground state singlet.

In contrast to $\mathcal{S}(^1\Sigma_g^{(a)})$ and $\mathcal{S}(^3\Sigma_u)$, $\mathcal{S}(^1\Sigma_g^{(b)})$ and $\mathcal{S}(^1\Sigma_u)$ are very sensitive to the asymmetry of the QDMs. In general, if the two dots have identical electronic structures (e.g., in the simple Hubbard model), $\mathcal{S}(^1\Sigma_g^{(b)}) = \mathcal{S}(^1\Sigma_g^{(a)})$ and $\mathcal{S}(^1\Sigma_u) = 1$,⁹ as is illustrated in Fig. 9(c) for $M_{\alpha'\alpha'}$. For $M_{\gamma\gamma}$, which is somehow asymmetric due to the strain and alloy effects, $\mathcal{S}(^1\Sigma_g^{(b)})$ is close to $\mathcal{S}(^1\Sigma_g^{(a)})$ at small d , and drops down at large d , whereas for $M_{\alpha\beta}$, $\mathcal{S}(^1\Sigma_g^{(b)})$ is different from $\mathcal{S}(^1\Sigma_g^{(a)})$ at all inter-dot distances. The slight asymmetry in $M_{\gamma\gamma}$ also causes $\mathcal{S}(^1\Sigma_u)$ to drop down at large d , similar to $\mathcal{S}(^1\Sigma_u)$ of $M_{\alpha\beta}$.

B. Degree of entanglement vs double occupation

Experimentally, it is very hard to measure the DOE of two electrons in the QDM directly, while it is relatively easy to measure the possibility of double occupation. Therefore it would be useful to explore the relation between DOE and the double occupation rate. The triplet states $^3\Sigma$ have negligible double occupation rate due to the Pauli exclusion principle. Here, we discuss the relation between DOE and double occupation rate for the ground state singlet $^1\Sigma_g^{(a)}$. We consider the simplest case, where only “s” orbital in each dot is considered. The ground state singlet $^1\Sigma_g^{(a)}$ wavefunction can

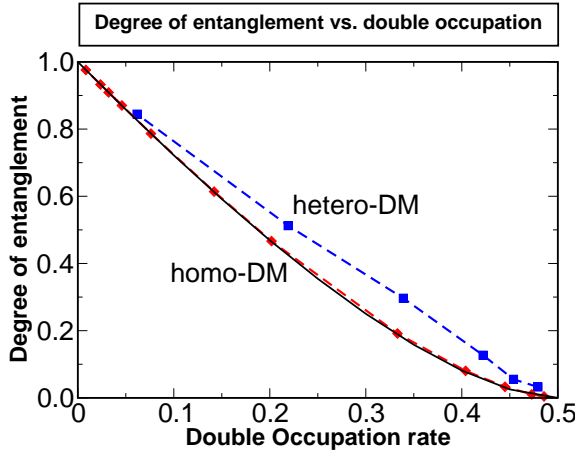


FIG. 10: (Color online) Comparison of the degree of entanglement *vs.* double occupation rate for hetero- and homo-QDMs. The black solid line represents the analytical results of homo-QDM, and the red dashed line represents the numerical results for homo-QDM $M_{\alpha'\alpha'}$, and $M_{\gamma\gamma}$, whereas the blue line represents the results for hetero-QDMs $M_{\alpha\beta}$.

be generally written as,

$$\Psi(^1\Sigma_g^{(a)}) = c_1|e_T^\uparrow, e_B^\downarrow\rangle + c_2|e_B^\uparrow, e_T^\downarrow\rangle + c_3|e_T^\uparrow, e_T^\downarrow\rangle + c_4|e_B^\uparrow, e_B^\downarrow\rangle, \quad (12)$$

and $|c_1|^2 + |c_2|^2 + |c_3|^2 + |c_4|^2 = 1$. Alternatively, we have

$$\Psi(^1\Sigma_g^{(a)}) = \sum_{i,j} \omega_{ij} |i\rangle \otimes |j\rangle \quad (13)$$

where,

$$\omega = \begin{pmatrix} 0 & -c_3 & 0 & -c_1 \\ c_3 & 0 & c_2 & 0 \\ 0 & -c_2 & 0 & -c_4 \\ c_1 & 0 & c_4 & 0 \end{pmatrix}, \quad (14)$$

and $|i\rangle, |j\rangle = |e_T^\uparrow\rangle, |e_T^\downarrow\rangle, |e_B^\uparrow\rangle, |e_B^\downarrow\rangle$. We can use Eq. 11 to calculate the DOE, where $z_1^2 = 1/2(1 - \sqrt{1 - 4(c_1c_2 - c_3c_4)^2})$ and $z_2^2 = 1/2(1 + \sqrt{1 - 4(c_1c_2 - c_3c_4)^2})$ are the eigenvalues of $\omega^\dagger \omega$. For a QDM with reflection symmetry, we have $c_1 = c_2$ and $c_3 = c_4$, and therefore $z_1^2 = 1/2(1 - \sqrt{1 - (1 - 4c_3^2)^2})$, and $z_2^2 = 1/2(1 + \sqrt{1 - (1 - 4c_3^2)^2})$. Using the definition of double occupation rate, $Q_{\text{tot}} = c_3^2 + c_4^2$, we have

$$\begin{aligned} z_1^2 &= 1/2(1 - \sqrt{1 - (1 - 2Q_{\text{tot}})^2}), \\ z_2^2 &= 1/2(1 + \sqrt{1 - (1 - 2Q_{\text{tot}})^2}). \end{aligned} \quad (15)$$

The DOE of $^1\Sigma_g^{(a)}$ is calculated by substituting z_1^2 , z_2^2 into Eq. (11). We plot the DOE *vs.* double occupation

rate of the above ideal model in Fig. 10 in a black solid line. We also present in the same figure, the DOE of $M_{\alpha\beta}$, $M_{\gamma\gamma}$ and $M_{\alpha'\alpha'}$ *vs.* double occupation rate. We found that the double occupation dependence of DOE for the homo-QDM $M_{\alpha'\alpha'}$ has perfect agreement with the analytical result, which is also true for $M_{\gamma\gamma}$ even though it has small asymmetry in the molecule due to the strain and alloy effects. We also checked the homo-QDM made of pure InAs/GaAs dots^{8,9}, and found the same double occupation dependence of DOE for the $^1\Sigma_g^{(a)}$ state, indicating this is a robust feature for homo-QDMs. However, the double occupation dependence of DOE for $M_{\alpha\beta}$ deviates from the ideal case because dots α and β are different.

VI. SUMMARY

We have studied the electronic structures of quantum dot molecules made of (In,Ga)As/GaAs dots of different sizes (hetero-QDMs), and compare them to that of quantum dot molecules made of identical dots (homo-QDMs). We found that while the hetero-QDMs and homo-QDMs have relatively similar electronic structures at short inter-dot distance, they differ significantly at large inter-dot distance. (i) Unlike those of homo-QDMs, the single-particle molecular orbitals of hetero-QDMs convert to dot localized orbitals at large inter-dot distance. (ii) Consequently, the bonding-antibonding splitting of molecular orbitals is significantly larger than the electron hopping energy in a hetero-QDM at large inter-dot distance, whereas for homo-QDM, the bonding-antibonding splitting is very similar to the hopping energy. (iii) The asymmetry of the QDM will significantly increase the double occupation for the two-electron ground states, and therefore lowers the degree of entanglement of the two electrons.

Acknowledgments

L. He acknowledges the support from the Chinese National Fundamental Research Program, the Innovation funds and “Hundreds of Talents” program from Chinese Academy of Sciences, and National Natural Science Foundation of China (Grant No. 10674124). The work done at NREL was funded by the U.S. Department of Energy, Office of Science, Basic Energy Science, Materials Sciences and Engineering, LAB-17 initiative, under Contract No. DE-AC36-99GO10337 to NREL.

¹ Q. Xie, A. Madhukar, P. Chen, and N. P. Kobayashi, Phys. Rev. Lett. **75**, 2542 (1995).

² G. S. Solomon, J. A. Trezza, A. F. Marshall, and J. S. Harris, Phys. Rev. Lett. **76**, 952 (1996).

³ M. Bayer, P. Hawrylak, K. Hinzer, S. Fafard, M. Korkusinski, Z. R. Wasilewski, O. Stern, and A. Forchel, Science **291**, 451 (2001).

⁴ D. Loss and D. P. DiVincenzo, Phys. Rev. A **57**, 120 (1998).

⁵ J. R. Petta, A. C. Johnson, C. M. Marcus, M. P. Hanson, and A. C. Gossard, Phys. Rev. Lett. **93**, 186802 (2004).

⁶ A. C. Johnson, J. R. Petta, C. M. Marcus, M. P. Hanson, and A. C. Gossard, Phys. Rev. B **72**, 165308 (2005).

⁷ G. Bester, J. Shumway, and A. Zunger, Phys. Rev. Lett. **93**, 047401 (2004).

⁸ L. He, G. Bester, and A. Zunger, Phys. Rev. B **72**, 081311(R) (2005).

⁹ L. He, G. Bester, and A. Zunger, Phys. Rev. B **72**, 195307 (2005).

¹⁰ M. C. Bödefeld, R. J. Warburton, K. Karrai, J. P. Kotthaus, G. Medeiros-Ribeiro, and P. M. Petroff, Appl. Phys. Lett. **74**, 1839 (1999).

¹¹ E. A. Stinaff, M. Scheibner, A. S. Bracker, I. V. Ponomarev, V. L. Korenev, M. E. Ware, M. F. Doty, T. L. Reinecke, and D. Gammon, Science **311**, 636 (2006).

¹² P. N. Keating, Phys. Rev. **145**, 637 (1966).

¹³ J. L. Martins and A. Zunger, Phys. Rev. B **30**, R6217 (1984).

¹⁴ A. J. Williamson, L.-W. Wang, and A. Zunger, Phys. Rev. B **62**, 12963 (2000).

¹⁵ L.-W. Wang and A. Zunger, Phys. Rev. B **59**, 15806 (1999).

¹⁶ A. Franceschetti, H. Fu, L.-W. Wang, and A. Zunger, Phys. Rev. B **60**, 1819 (1999).

¹⁷ M. Rontani, F. Troiani, U. Hohenester, and E. Molinari, Solid State Comm. **119**, 309 (2001).

¹⁸ C. Edmiston and K. Ruedenberg, Rev. Mod. Phys. **35**, 457 (1963).

¹⁹ T. Ota, M. Rontani, S. Tarucha, Y. Nakata, H. Z. Song, T. Miyazawa, T. Usuki, M. Takatsu, and N. Yokoyama, Phys. Rev. Lett. **95**, 236801 (2005).

²⁰ M. A. Nielsen and I. L. Chuang, *Quantum Computation and Quantum Information* (Cambridge University Press, Cambridge, 2000).

²¹ C. H. Bennett, H. J. Bernstein, S. Popescu, and B. Schumacher, Phys. Rev. A **53**, 2046 (1996).

²² C. H. Bennett, D. P. DiVincenzo, J. A. Smolin, and W. K. Wootters, Phys. Rev. A **54**, 3824 (1996).

²³ A. Wehr, Rev. Mod. Phys. **50**, 221 (1978).

²⁴ J. Schliemann, J. I. Cirac, M. Kuś, M. Lewenstein, and D. Loss, Phys. Rev. A **64**, 022303 (2001).

²⁵ R. Paškauskas and L. You, Phys. Rev. A **64**, 042310 (2001).

²⁶ Y. S. Li, B. Zeng, X. S. Liu, and G. L. Long, Phys. Rev. A **64**, 054302 (2001).

²⁷ P. Zanardi, Phys. Rev. A **65**, 042101 (2002).

²⁸ Y. Shi, Phys. Rev. A **67**, 24301 (2003).

²⁹ H. M. Wiseman and J. A. Vaccaro, Phys. Rev. Lett. **91**, 097902 (2003).

³⁰ G. C. Ghirardi and L. Marinatto, Phys. Rev. A **70**, 012109 (2004).

³¹ C. N. Yang, Rev. Mod. Phys. **34**, 694 (1962).